A complete solar coronal loop stability analysis in ideal magnetohydrodynamics

I. Non-force-free cylindrical equilibria

R.A.M. Van der Linden[1,*] **and A.W. Hood**[2]

[1] Center for Plasma Astrophysics, Katholieke Universiteit Leuven, Celestijnenlaan 200B, B-3001 Leuven, Belgium
[2] School of Mathematical and Computational Sciences, University of St. Andrews, St. Andrews KY16 9SS, UK

Abstract. A procedure is introduced to perform a complete ideal MHD stability analysis of one-dimensional cylindrical equilibrium models for coronal loops, including the important effect of line-tying. The stability is completely determined by calculating the critical (marginally stable) length for the onset of ideal MHD instabilities for every azimuthal wave number m. The analysis consists of the combination of a WKB method to determine the critical length of intermediate to high (infinite) values of m with a numerical code (using bicubic finite elements) for the low to intermediate values of m. As before it is found that for large enough m the critical length can be expressed as $l_c = l_0 + l_1/m$. It is also demonstrated that in general either the $m = 1$ or the $m \to \infty$ mode has the shortest critical length, the former being the first to become unstable for nearly force-free magnetic fields, the latter for strongly non-force-free fields. Therefore, a stability analysis of these two modes will normally suffice, with perhaps a need for some more numerical calculations near the point where the modes cross over. The combination of these two tools provides a complete stability assessment.

Key words: MHD – plasmas – Sun: corona – Sun: magnetic fields

1. Introduction

Most of the solar coronal plasma exists in the form of coronal loops of various sizes, which have often been termed 'the building blocks of the solar corona'. Evidently then, the question of the (long-term) stability of these solar coronal loops, and the point of onset of instability (leading to loop brightening or a complete disruption of the equilibrium) is very important. The stability of many classes of equilibrium models of coronal loops has therefore been studied by a large number of authors (see e.g. Hood (1992) for an overview). This stability assessment is most economically done using the linearised equations

Send offprint requests to: R.A.M. Van der Linden
* Postdoctoral Research Fellow of the Flemish Fund for Scientific Research

for small perturbations. At the same time, linear studies provide useful information to assist subsequent non-linear calculations.

Previous stability assessments of coronal loops have been mostly numerical, and were therefore limited to global modes of instability. In the straight cylindrical approximation usually taken, nearly all calculations only considered $m = 1$ kink mode instabilities, largely because this mode is generally considered to be the most 'dangerous', or relevant, in the classic literature on stability of infinite one-dimensional cylindrical magnetic equilibria (e.g. Newcomb (1960)). An essential ingredient in the stability study of solar coronal loops, however, is the stabilising influence of the anchoring of magnetic field lines to the dense photosphere, *line-tying*. Including this, usually in the form of boundary conditions at the interface between corona and photosphere, makes the analysis two-dimensional, and most results from the classic literature on the stability of one-dimensional cylindrical equilibria are not valid or become irrelevant in this context. Also, it no longer holds that it is sufficient to investigate the stability of the $m = 1$ mode only, because it has been shown that when line-tying is included, equilibria exist in which high-m modes become unstable first, i.e. for shorter loop lengths (Hood et al. (1994)). Hence, a full stability assessment needs to be able to determine the stability boundaries of *all* modes, including both the very global low-m and the highly localised high-m modes. This requires a combination of both numerical and analytical techniques.

The development of such a *complete stability assessment* was started in Hood et al. (1994), where *unsheared* magnetic fields were considered. In this paper, we present the generalisation of this work to arbitrary one-dimensional, cylindrically symmetric equilibrium models of line-tied coronal loops. As before, the approach is largely based on the method of Connor et al. (1979). Only the case of non-force-free equilibria is presented here, since it was found that the scalings for sheared force-free equilibria are completely different than those in the other cases, so that significant modifications to the method are required. Work on these classes of equilibria is still in progress and will be detailed in a subsequent paper. Some reference will however be made to preliminary results, as these are relevant

for instabilities with low mode numbers m in nearly-force-free equilibria.

While in the simpler constant-twist equilibria studied in Hood et al. (1994) the WKB equations could be solved entirely analytically (at worst the roots of a transcendental algebraic equation had to be determined), this is only formally the case in more general equilibria (solutions can still be expressed in terms of Legendre functions, but this is of little practical use). Still, the WKB method only requires solving a simple ordinary differential equation over a range of parameters rather than the far more complicated two-dimensional partial differential equations.

To be able to determine the stability boundaries of low-m modes, the WKB method is complemented with a newly developed numerical stability code, using bicubic finite elements to solve the full set of two-dimensional partial differential equations. It is demonstrated that this code has far better convergence properties than the Fourier series methods employed before by a number of authors (Einaudi and Van Hoven 1983, Van der Linden et al. 1990, Velli et al. 1990, De Bruyne and Hood 1992, Hood et al. 1994, Van der Linden and Hood 1995). The flexibility of the finite element numerical technique and the use of (two choices of) an eikonal or 'ballooning' factor in the numerical solution of the partial partial differential equations makes it possible to obtain a large overlap region where the accuracy obtained with the numerical code is sufficient and at the same time the WKB method yields reasonable approximations. Thus, the consistency of the two methods can at all times be thoroughly checked, and very good agreement is found between them.

2. Marginal stability equations

The equations used as the starting point in this paper have already been specified in Hood et al. (1994), and are repeated here for completeness. From a physical point of view the main interest is in determining the point at which the, by assumption, slowly evolving equilibrium first becomes unstable. This point is found by solving the marginal stability equations, which are obtained from the well-known equation of motion in linearised ideal MHD by setting the derivatives with respect to time equal to zero:

$$\nabla(\boldsymbol{\xi} \cdot \nabla p + \gamma p \nabla \cdot \boldsymbol{\xi}) + \frac{[\nabla \times (\nabla \times (\boldsymbol{\xi} \times \boldsymbol{B}))]}{\mu} \times \boldsymbol{B}$$
$$+ \frac{\nabla \times \boldsymbol{B}}{\mu} \times [\nabla \times (\boldsymbol{\xi} \times \boldsymbol{B})] = 0, \tag{1}$$

where $\boldsymbol{\xi}$ is the displacement vector, p and $\boldsymbol{B}$ are the equilibrium gas pressure and magnetic field respectively, and μ is the magnetic permeability. The ratio of specific heats, γ, is set equal to $5/3$ throughout the paper.

We model coronal loops by a straight cylindrical equilibrium

$$\boldsymbol{B} = (0, B_\theta(r), B_z(r)), \quad p = p(r), \tag{2}$$

where (r, θ, z) are the usual cylindrical coordinates. For illustration of the WKB method and comparison with numerical solutions we take an equilibrium constructed by
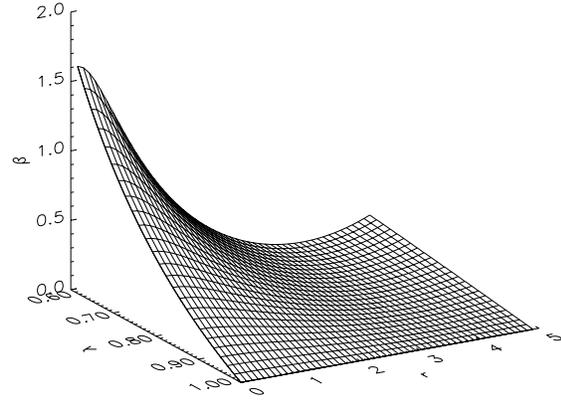

Fig. 1. The ratio of gas to magnetic pressure ($\beta = 2\mu p/B^2$) of the equilibrium (3) as a function of r and λ, fixing $\sigma = 0.15$.

Cargill et al. (1986), who generalised a form first used in Anzer (1968):

$$B_\theta = r \exp(-r/2),$$
$$B_z = \lambda \sqrt{\sigma + (2 + 2r - r^2) \exp(-r)}, \tag{3}$$
$$\mu p = \frac{1}{2} (1 - \lambda^2) \left[\sigma + (2 + 2r - r^2) \exp(-r) \right],$$

where r now represents the dimensionless radial distance, and λ and σ are parameters (unless otherwise specified, all numerical examples in this paper refer to the above equilibrium with $\sigma = 0.15$). This equilibrium was selected mainly because it has been used by a number of authors in the past to model coronal loops and arcades, and to determine the stability of global modes (i.e. modes with low values of the azimuthal wave number m). Unlike the Gold-Hoyle equilibrium considered in Hood et al. (1994), equilibrium (3) has shear, i.e. the twist $q = rB_\theta/B_z$ is a function of the radial distance, which is why this type of equilibrium requires a more general treatment. To indicate the characteristics of the present class of equilibrium, we have plotted the plasma β and the twist profile in Figs. 1 and 2 respectively.

Particular attention is drawn to the fact that the twist reaches a minimum for this equilibrium (see Fig. 2), which turns out to be of particular relevance when the equilibrium is close to its force-free state, since the instabilities then become localised near that point. This will be discussed in detail in a subsequent paper.

Writing the displacement in terms of its components in the radial, parallel (to $\boldsymbol{B}$) and perpendicular directions, i.e.

$$\boldsymbol{\xi} = \left(\xi_r, \frac{-\zeta B_z}{B^2} + \eta \frac{B_\theta}{B^2}, \frac{\zeta B_\theta}{B^2} + \frac{\eta B_z}{B^2} \right), \tag{4}$$

we can rewrite Eq. (1) as

$$\mathcal{L}\zeta = \mathcal{M}\xi_r' + \mathcal{N}\xi_r + \frac{\gamma \mu p}{B^2} \mathcal{M}(\nabla \cdot \boldsymbol{\xi}), \tag{5}$$

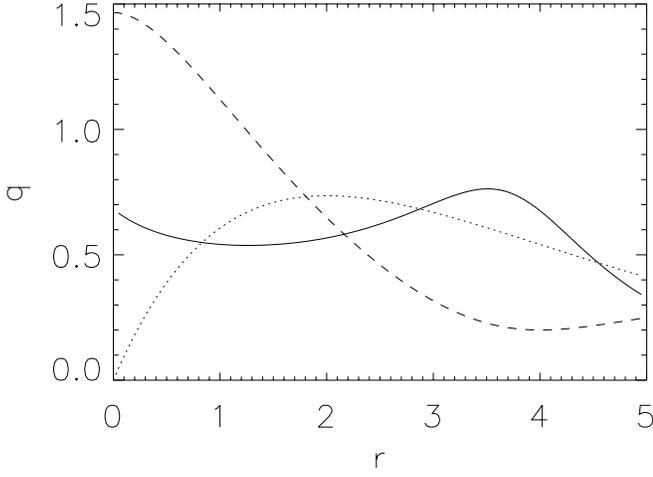$$\gamma \mu p (\boldsymbol{B} \cdot \nabla) (\nabla \cdot \boldsymbol{\xi}) = 0, \tag{6}$$

Fig. 2. Radial profiles of the magnetic field components B_z (dashed) and B_θ (dotted) and the magnetic twist $q = rB_z/B_\theta$ for equilibrium (3) for $\sigma = 0.15$ and $\lambda = 1.0$. For other values of λ the profiles of B_z and q are obtained from the present ones by simply scaling down, while B_θ remains unchanged.

$$\frac{1}{r}(rB^2\xi_r')' + \left[(\boldsymbol{B}\cdot\nabla)^2 + \frac{2B_zB_z'}{r} + \frac{B_\theta^2 - B_z^2}{r^2}\right]\xi_r =$$

$$= (\mathcal{M}\zeta)' - 2\frac{B_\theta}{r}\frac{\partial\zeta}{\partial z} - (\gamma\mu p\nabla\cdot\boldsymbol{\xi})', \tag{7}$$

where

$$\nabla\cdot\boldsymbol{\xi} = \frac{(\boldsymbol{B}\cdot\nabla)\,\eta}{B^2} - \frac{\mathcal{M}\zeta}{B^2} + \xi_r' + \frac{\xi_r}{r}, \tag{8}$$

a dash denotes differentiation with respect to r and the differential operators are defined as

$$\mathcal{L} = \frac{1}{r^2}\frac{\partial^2}{\partial\theta^2} + \frac{\partial^2}{\partial z^2} = \frac{\mathcal{M}^2}{B^2} + \frac{(\boldsymbol{B}\cdot\nabla)^2}{B^2}, \tag{9}$$

$$\mathcal{M} = \frac{B_z}{r}\frac{\partial}{\partial\theta} - B_\theta\frac{\partial}{\partial z}, \tag{10}$$

$$\mathcal{N} = \frac{1}{r}\left(\frac{B_z}{r}\frac{\partial}{\partial\theta} + B_\theta\frac{\partial}{\partial z}\right). \tag{11}$$

Photospheric line-tying is modelled using rigid wall boundary conditions, as these have been shown to yield the best representation of the stabilising effect of the anchoring of magnetic field lines in the dense photospheric plasma (Hood, 1986, Van der Linden et al., 1994)

$$\xi_r = \zeta = \eta = 0 \quad \text{at } z = \pm\ell, \tag{12}$$

where we have introduced the half-length ℓ of the loop. The radial boundary conditions are $r\xi_r = 0$ at $r = 0$ and $r \to \infty$.

The problem that needs to be solved now is to determine ℓ for the *most unstable* mode in a given equilibrium profile, i.e. to find the smallest ℓ for which a solution to the above set of partial differential equations (PDE) and boundary conditions exists. In practice, this means we need to determine ℓ for the fundamental harmonic only in the radial (r) coordinate, but we need to consider all possible values of the azimuthal wave number m, since

it is not a priori obvious which m yields the most unstable mode (in fact, it was shown in Hood et al. (1994) that depending on the equilibrium, either $m = 1$ or $m \to \infty$ can be the most unstable mode). As is well-known (see, e.g., Newcomb (1960)), for a given m, the z-dependence of the most unstable mode will be such that the field line bending is minimised, i.e. the most unstable harmonic in the z coordinate is the one which generates a perturbation that follows the field lines as closely as possible.

3. Application of the WKB method

As in Hood et al. (1994), we first eliminate the perpendicular component ζ of the displacement vector. Expressions for ζ and ζ' in terms of $(\gamma\mu p\nabla\cdot\boldsymbol{\xi})'$, $\gamma\mu p\nabla\cdot\boldsymbol{\xi}$, ξ_r'', ξ_r' and ξ_r are obtained from Eq. (5) and $\mathcal{L}$ operating on the radial derivative of Eq. (5). Operating with $\mathcal{L}^2$ on Eq. (7) and substituting the expressions for ζ and its derivatives then gives the equation for ξ_r as

$$\mathcal{L}(\boldsymbol{B}\cdot\nabla)^2\xi_r'' + \left\{\frac{\mathcal{L}}{r}\left[r(\boldsymbol{B}\cdot\nabla)^2\right]' - \mathcal{L}'(\boldsymbol{B}\cdot\nabla)^2\right\}\xi_r'$$

$$+ \left\{\mathcal{L}^2(\boldsymbol{B}\cdot\nabla)^2 - \frac{2p'}{r}\mathcal{L}\frac{\partial^2}{\partial z^2} + \frac{\mathcal{L}}{r^2}(\boldsymbol{B}\cdot\nabla)^2\right.$$

$$\left. + \frac{2}{r^2}\frac{\partial^2}{\partial z^2}\left[\boldsymbol{B}\cdot\nabla\left(\frac{B_\theta}{r}\frac{\partial}{\partial\theta} - B_z\frac{\partial}{\partial z}\right)\right]\right\}\xi_r$$

$$+ 2\frac{B_\theta}{rB^4}\left(\frac{B_z}{r}\frac{\partial}{\partial\theta} - B_\theta\frac{\partial}{\partial z}\right)^3\frac{\partial}{\partial z}(\gamma\mu p\nabla\cdot\boldsymbol{\xi}) = 0. \tag{13}$$

The second equation is still Eq. (6) with ζ substituted in expression (8) for $\nabla\cdot\boldsymbol{\xi}$.

Closely following the method outlined by Connor et al. (1979), we introduce the eikonal factor

$$\xi_r(r,\theta,z) = \tilde{\xi}(r,z)\exp\{im[\theta - q(z - z_0)]\},$$

$$\eta(r,\theta,z) = \tilde{\eta}(r,z)\exp\{im[\theta - q(z - z_0)]\}, \tag{14}$$

where $q = B_\theta/rB_z$ and the wave number m in the θ coordinate must be an integer to give periodic solutions. Here, the exponential factor ensures that the mode follows the field lines and the strongly stabilising effect of field line bending is minimised. The remaining slow variation along the field lines and the radial dependence of the eigenmodes are given by the amplitude functions $\tilde{\xi}$ and $\tilde{\eta}$ (in the following we will drop the tildes).

After substitution of (14) into the differential equations, the azimuthal wave number m enters as a parameter in the resulting PDE. For sufficiently large m approximate analytical solutions can then be constructed using the WKB method (see e.g. Bender and Orszag (1978) for a detailed description). In this method, both the solutions and the equations are expanded in powers of the large (or small) parameter and solutions are constructed at every order separately. The method becomes more accurate as m gets larger, but obviously breaks down when m is too small.

Redefining the longitudinal coordinate

$$z = \ell\bar{z}, \tag{15}$$

brings out explicitly the quantity ℓ to be determined. We then set, as in Hood et al. (1994) and following Connor et al. (1979),

$$x = m^{1/2}(r - r_0), \qquad \ell = \ell_0 + \frac{1}{m}\ell_1 + \frac{1}{m^2}\ell_2 + \cdots, \qquad (16)$$

where r_0 is the (as yet undetermined) position about which the modes become localised as $m \to \infty$, and expand the eigenfunctions as

$$\xi = \xi_0(x, \bar{z}) + \frac{1}{m^{1/2}}\xi_1(x, \bar{z}) + \frac{1}{m}\xi_2(x, \bar{z}) + \ldots, \qquad (17)$$

$$\eta = \eta_0(x, \bar{z}) + \frac{1}{m^{1/2}}\eta_1(x, \bar{z}) + \frac{1}{m}\eta_2(x, \bar{z}) + \ldots. \qquad (18)$$

Substituting into the marginal stability equations, Eqs. (13) and (6), we get to leading order, $\mathcal{O}(m^4)$,

$$\mathcal{L}_0(\xi_0, \eta_0) \equiv -\frac{\partial}{\partial \bar{z}}\left\{\left[\frac{a}{\ell_0^2} + d\,(\bar{z} - \bar{z}_0)^2\right]\frac{\partial \xi_0}{\partial \bar{z}}\right\} + b\xi_0$$
$$+ c\left[\frac{\partial \eta_0}{\partial \bar{z}} + \xi_0\right] = 0, \qquad (19)$$

and

$$\frac{\partial}{\partial \bar{z}}\left[\frac{\partial \eta_0}{\partial \bar{z}} + \xi_0\right] = 0, \qquad (20)$$

where the coefficients

$$a = B^2/r^2, \qquad\qquad b = 2p'B_\theta^2/r^3 B_z^2,$$
$$c = 4\gamma\mu p B_\theta^4/r^4 B_z^2(\gamma\mu p + B^2), \qquad d = B_z^2 q'^2,$$

are all evaluated at $r = r_0$, and η has been redefined as

$$\frac{rB_z\eta}{2B_\theta^2 \ell} \to \eta. \qquad (21)$$

For unsheared equilibria $q' \equiv 0$, giving $d = 0$ and the leading order equations of Hood et al. (1994) are recovered. Due to the presence of $\bar{z}$ in Eq. (19) solutions in the present case are no longer as simple as in Hood et al. (1994).

Eq. (20) can be integrated once and the result substituted in Eq. (19) to yield

$$-\frac{\partial}{\partial z}\left\{\left[\frac{a}{\ell_0^2} + d\,(\bar{z} - \bar{z}_0)^2\right]\frac{\partial \xi_0}{\partial z}\right\} + b\xi_0 + c\alpha = 0, \qquad (22)$$

where α is the integration constant. The homogeneous part of this equation can be written as the standard equation for Legendre functions, so we can formally write the solution as

$$\xi_0 = AP_\nu\left(-\frac{i\ell_0\sqrt{d}}{\sqrt{a}}(\bar{z} - \bar{z}_0)\right)$$
$$+ BQ_\nu\left(-\frac{i\ell_0\sqrt{d}}{\sqrt{a}}(\bar{z} - \bar{z}_0)\right) - \frac{c\alpha}{b}, \qquad (23)$$

where P_ν and Q_ν are the Legendre functions of order 0 and degree ν, with ν one of the two equivalent solutions to

$$\nu(\nu + 1) = \frac{b}{d}. \qquad (24)$$

The boundary conditions $\xi_0(\bar{z} = \pm 1) = 0$ provide expressions for A and B in terms of α. Then, solving for η by integrating Eq. (20), and applying the line-tying boundary conditions then results in the condition

$$A \int_{-1}^{1} P_\nu\left(-\frac{i\ell_0\sqrt{d}}{\sqrt{a}}(\bar{z} - \bar{z}_0)\right)\mathrm{d}z$$
$$+ B \int_{-1}^{1} Q_\nu\left(-\frac{i\ell_0\sqrt{d}}{\sqrt{a}}(\bar{z} - \bar{z}_0)\right)\mathrm{d}z - \frac{2c\alpha}{b} + 2\alpha = 0, \quad (25)$$

which defines the critical (marginal) length ℓ_0 as a function of r_0 and $\bar{z}_0$. Eq. (25) is however of little practical use, since ν is in general not an integer, and therefore no simple expression for the Legendre functions can be given. In practice therefore, the ordinary differential equations (19) and (20) are solved numerically to determine $\ell_0 = \ell_0(r_0, z_0)$.

The next order equations, $\mathcal{O}(m^{7/2})$, in the expansion of Eqs. (13) and (6) are given by

$$\mathcal{L}_0(\xi_1, \eta_1) + x\left(\frac{\partial \mathcal{L}_0}{\partial r_0}\right)(\xi_0, \eta_0)$$
$$+ \frac{i}{\ell_0 q'}\left(\frac{\partial \mathcal{L}_0}{\partial \bar{z}_0}\right)\frac{\partial}{\partial x}(\xi_0, \eta_0) = 0, \qquad (26)$$

and

$$\frac{\partial}{\partial \bar{z}}\left[\frac{\partial \eta_1}{\partial \bar{z}} + \xi_1\right] = 0, \qquad (27)$$

where $\frac{\partial \mathcal{L}_0}{\partial r_0}$ and $\frac{\partial \mathcal{L}_0}{\partial \bar{z}_0}$ are the differential operators obtained by differentiating the coefficients in $\mathcal{L}_0$ with respect to r_0 and $\bar{z}_0$ respectively. Using derivatives with respect to r_0 and z_0 of the leading order Eqs. (19), (20), we can rewrite Eq. (26) as

$$\mathcal{L}_0(\xi_1, \eta_1) = x\mathcal{L}_0\left(\frac{\partial \xi_0}{\partial r_0}, \frac{\partial \eta_0}{\partial r_0}\right) + x\frac{2a}{l_0^3}\frac{\partial \ell_0}{\partial r_0}\frac{\partial^2 \xi_0}{\partial \bar{z}^2}$$
$$- \frac{i}{q'\ell_0}\frac{\partial}{\partial x}\left[\mathcal{L}_0\left(\frac{\partial \xi_0}{\partial \bar{z}_0}, \frac{\partial \eta_0}{\partial \bar{z}_0}\right) + \frac{2a}{\ell_0^3}\frac{\partial \ell_0}{\partial \bar{z}_0}\frac{\partial^2 \xi_0}{\partial \bar{z}^2}\right]. \quad (28)$$

Multiplying this equation with ξ_0, and using integration by parts (or actually the fact that $\mathcal{L}_0$ is a Hermitian operator), and applying Eqs. (19) and (20) then immediately results in the conditions

$$\frac{\partial \ell_0}{\partial \bar{z}_0} = \frac{\partial \ell_0}{\partial r_0} = 0, \qquad (29)$$

i.e. both $\bar{z}_0$ and r_0 must be selected at the minimum of ℓ_0. From symmetry it is actually obvious that $\bar{z}_0 = 0$, but the value of r_0 must be determined from the (numerical) solutions of the leading-order equations.

Finally, in order to determine the correction to the marginal stability length (for large but finite m) we use the $\mathcal{O}(m^3)$ equations:

$$\mathcal{L}_0(\xi_2, \eta_2) + x\left(\frac{\partial \mathcal{L}_0}{\partial r_0}\right)(\xi_1, \eta_1) + \frac{x^2}{2}\left(\frac{\partial^2 \mathcal{L}_0}{\partial r_0^2}\right)(\xi_0, \eta_0)$$
$$+ \frac{i}{\ell_0 q'}\left(\frac{\partial \mathcal{L}_0}{\partial \bar{z}_0}\right)\frac{\partial}{\partial x}(\xi_1, \eta_1)$$

$$+ x \left[\frac{\partial}{\partial r_0} \left(\frac{i}{\ell_0 q'} \frac{\partial \mathcal{L}_0}{\partial \bar{z}_0} \right) \right] \frac{\partial}{\partial x} (\xi_0, \eta_0)$$

$$- \frac{1}{2\ell_0^2 q'^2} \left(\frac{\partial^2 \mathcal{L}_0}{\partial \bar{z}_0^2} \right) \frac{\partial^2}{\partial x^2} (\xi_0, \eta_0)$$

$$+ \ell_1 \frac{2a}{\ell_0^3} \frac{\partial^2 \xi_0}{\partial \bar{z}^2} + \mathcal{L}_{2a}(\xi_0, \eta_0) = 0, \tag{30}$$

and

$$\frac{\partial}{\partial \bar{z}} \left[\frac{\partial \eta_2}{\partial \bar{z}} + \xi_2 + \mathcal{L}_{2b}(\xi_0, \eta_0) \right] = 0. \tag{31}$$

Here the operators $\mathcal{L}_{2a,b}$ are defined by

$$\mathcal{L}_{2b}(\xi_0, \eta_0) = \frac{irB_z^3}{B_\theta B^2} \frac{\partial \xi_0}{\partial \bar{z}} + \frac{iq'r^3 B_z^4}{2B_\theta^2 B^2} \frac{\partial^2}{\partial \bar{z}^2} [(\bar{z} - \bar{z}_0)\xi_0],$$

$$\mathcal{L}_{2a}(\xi_0, \eta_0) = c\mathcal{L}_{2b}(\xi_0, \eta_0)$$

$$+ i \left(q''B_z^2 + \frac{3q'B_z^4}{rB^2} + 2q'B_z B_z' + \frac{B_\theta^2 B_z^2 q'}{rB^2} \right.$$

$$\left. - 4q'^2 \frac{rB_\theta B_z^3}{B^2} \right) \frac{\partial^2}{\partial \bar{z}^2} [(\bar{z} - \bar{z}_0) \xi_0]$$

$$+ \frac{2irB_\theta B_z^3 q'^2}{B^2} \frac{\partial^3}{\partial \bar{z}^3} [(\bar{z} - \bar{z}_0) \xi_0]$$

$$+ \frac{4iB_\theta B_z}{r} \frac{\partial^3 \xi_0}{\partial \bar{z}^3} - 4i \left(\frac{B_\theta^3 B_z}{r^3 B^2} + \frac{p'B_\theta B_z}{r^2 B^2} \right) \frac{\partial \xi_0}{\partial \bar{z}}.$$

As before, we obtain a solvability condition by multiplying Eq. (30) with ξ_0 and integrating over $\bar{z}$. Since we need to evaluate the expressions at the minimum of $\ell_0(r_0, z_0)$, we must take $z_0 = 0$, and since we are considering the most unstable mode (for which ξ_0 is even about $\bar{z} = 0$), the contributions from $\mathcal{L}_{2a}(\xi_0, \eta_0)$ are odd and integrate to 0. For the same reason the fifth term in Eq. (30) can be discarded. From the self-adjointness of $\mathcal{L}_0$ and Eqs. (19)-(20) it is clear that the first term in Eq. (30) also integrates to zero. We thus obtain the integrability condition

$$x \int_{-1}^{1} \xi_0 \left(\frac{\partial \mathcal{L}_0}{\partial r_0} \right) (\xi_1, \eta_1) \mathrm{d}\bar{z} + \frac{x^2}{2} \int_{-1}^{1} \xi_0 \left(\frac{\partial^2 \mathcal{L}_0}{\partial r_0^2} \right) (\xi_0, \eta_0) \mathrm{d}\bar{z}$$

$$+ \frac{i}{\ell_0 q'} \int_{-1}^{1} \xi_0 \left(\frac{\partial \mathcal{L}_0}{\partial \bar{z}_0} \right) \frac{\partial}{\partial x} (\xi_1, \eta_1) \mathrm{d}\bar{z}$$

$$- \frac{1}{2\ell_0^2 q'^2} \int_{-1}^{1} \xi_0 \left(\frac{\partial^2 \mathcal{L}_0}{\partial \bar{z}_0^2} \right) \frac{\partial^2}{\partial x^2} (\xi_0, \eta_0) \mathrm{d}\bar{z}$$

$$+ \ell_1 \frac{2a}{\ell_0^3} \int_{-1}^{1} \xi_0 \frac{\partial^2 \xi_0}{\partial \bar{z}^2} \mathrm{d}\bar{z} = 0. \tag{32}$$

Using several integrations by parts, Eqs. (19), (20), (26), (27) and the derivative with respect to r_0 of Eq. (19), we find

$$\int_{-1}^{1} \xi_0 \left(\frac{\partial \mathcal{L}_0}{\partial r_0} \right) (\xi_1, \eta_1) \mathrm{d}\bar{z} =$$

$$= x \int_{-1}^{1} \xi_0 \left(\frac{\partial \mathcal{L}_0}{\partial r_0} \right) \left(\frac{\partial \xi_0}{\partial r_0}, \frac{\partial \eta_0}{\partial r_0} \right) \mathrm{d}\bar{z}. \tag{33}$$

Similarly one can show that

$$\int_{-1}^{1} \xi_0 \left(\frac{\partial \mathcal{L}_0}{\partial \bar{z}_0} \right) \frac{\partial}{\partial x} (\xi_1, \eta_1) \mathrm{d}\bar{z} =$$

$$= \frac{i}{\ell_0 q'} \int_{-1}^{1} \frac{\partial \xi_0}{\partial \bar{z}_0} \left(\frac{\partial \mathcal{L}_0}{\partial \bar{z}_0} \right) \left(\frac{\partial^2 \xi_0}{\partial x^2}, \frac{\partial^2 \eta_0}{\partial x^2} \right) \mathrm{d}\bar{z}, \tag{34}$$

upon using $\partial/\partial r_0$ of Eq. (19) and $\partial/\partial x$ of Eq. (26). After further integrations by parts, Eq. (32) becomes

$$- \frac{1}{2\ell_0^2 q'^2} \int_{-1}^{1} \frac{\partial^2 \xi_0}{\partial x^2} \left[\left(\frac{\partial^2 \mathcal{L}_0}{\partial \bar{z}_0^2} \right) (\xi_0, \eta_0) \right.$$

$$\left. + 2 \left(\frac{\partial \mathcal{L}_0}{\partial \bar{z}_0} \right) \left(\frac{\partial \xi_0}{\partial \bar{z}_0}, \frac{\partial \eta_0}{\partial \bar{z}_0} \right) \right] \mathrm{d}\bar{z}$$

$$+ \frac{x^2}{2} \int_{-1}^{1} \xi_0 \left[\left(\frac{\partial^2 \mathcal{L}_0}{\partial r_0^2} \right) (\xi_0, \eta_0) + 2 \left(\frac{\partial \mathcal{L}_0}{\partial r_0} \right) \left(\frac{\partial \xi_0}{\partial r_0}, \frac{\partial \eta_0}{\partial r_0} \right) \right] \mathrm{d}\bar{z}$$

$$+ \ell_1 \frac{2a}{\ell_0^3} \int_{-1}^{1} \xi_0 \frac{\partial^2 \xi_0}{\partial \bar{z}^2} \mathrm{d}\bar{z} = 0. \tag{35}$$

Finally, using the second order derivatives with respect to $\bar{z}_0$ and r_0 of the leading order equation, Eq. (19), we obtain

$$\int_{-1}^{1} \left[\ell_1 \xi_0 + \frac{1}{2\ell_0^2} \frac{\partial^2 \ell_0}{\partial \bar{z}_0^2} \frac{\partial^2 \xi_0}{\partial x^2} - \frac{x^2}{2} \frac{\partial^2 \ell_0}{\partial r_0^2} \xi_0 \right] \frac{\partial^2 \xi_0}{\partial \bar{z}^2} \mathrm{d}z = 0. \tag{36}$$

From this it follows immediately that the x-dependence of ξ_0 is determined by the usual equation

$$\frac{\partial^2 \xi_0}{\partial x^2} + (\Lambda - \mu^2 x^2) \xi_0 = 0, \tag{37}$$

with

$$\Lambda = 2\ell_0^2 q'^2 \ell_1 \left(\frac{\partial^2 \ell_0}{\partial \bar{z}_0^2} \right)^{-1} \tag{38}$$

and

$$\mu^2 = \ell_0^2 q'^2 \left(\frac{\partial^2 \ell_0}{\partial r_0^2} \right) \left(\frac{\partial^2 \ell_0}{\partial \bar{z}_0^2} \right)^{-1}, \tag{39}$$

which has as (fundamental) solution

$$\xi_0 = e^{-\mu x^2/2}, \tag{40}$$

for $\Lambda = \mu$. Thus, the correction to the marginal stability length is given by

$$\ell_1 = \frac{1}{2\ell_0 |q'|} \sqrt{\left(\frac{\partial^2 \ell_0}{\partial r_0^2} \right) \left(\frac{\partial^2 \ell_0}{\partial \bar{z}_0^2} \right)}. \tag{41}$$

4. Numerical solutions and comparison with WKB results

In Hood et al. (1994), the WKB results for shearless magnetic fields were compared with numerical solutions obtained using a code that combines a finite element discretisation in the radial direction with a Fourier series expansion in the z coordinate (see also Van der Linden et al. 1990). It was noted however that the convergence rate in terms of the number of Fourier components taken was rather slow, the reason being that the expansion functions themselves do not satisfy the boundary conditions, but are periodic instead (while the variables used are not). In practice therefore, even using fairly high numbers of Fourier modes on its own doesn't give sufficiently accurate results to allow a meaningful comparison with the WKB estimates. The only option then was to use an extrapolation procedure to try and estimate the converged values (i.e. those one would get with an infinite number of terms in the Fourier series) of the marginal stability length. Obviously, this undesirable additional procedure may produce unreliable results. Therefore, a new code, named MALTS (MArginal Line-Tied Stability), was constructed to generate more accurate (converged) marginal stability lengths and to allow a more straightforward comparison with the WKB method. This new code is described in the Appendix.

To illustrate the improvement obtained by going from the old numerical code using a Fourier series to the new bicubic finite elements code MALTS, a convergence study was done for a particular illustrative example, calculating the $m = 10$ mode in the equilibrium specified in Eq. (3), for $\lambda = 0.6$ and $\sigma = 0.15$. The results are shown in Fig. 3, where we plot the calculated marginal stability length versus the number of expansion coefficients per gridpoint (in the r coordinate) per variable. Although the comparison may be somewhat simplistic, Fig. 3 does clearly indicate that the bicubic code gives superior results, and in particular eliminates the need for the extrapolation procedure to the limit of an infinite number of expansion coefficients.

We now concentrate specifically on the equilibrium given by Eq. (3) to verify agreement between the numerical results and the WKB analysis, and to demonstrate how the combination of the two gives a complete stability assessment of the equilibrium in question. First of all, we fix the parameters of the equilibrium to $\lambda = 0.6, \sigma = 0.15$. We use a simple code to solve the ordinary differential equations (19)-(20) numerically in order to get the WKB estimate $\ell_0 + \ell_1/m$ as explained in the previous section. We find

$$\ell_0 = 2.55949, \qquad \ell_1 = 0.545751. \qquad (42)$$

These WKB results are compared with numerically obtained values over a range of m in Table 1, which demonstrates very good agreement indeed. For a more detailed interpretation of Table 1, it is important to point out that all the numerical solutions were obtained using the same size (44×35) mesh. Even though the radial width of the computational domain was decreased as m increased (to reflect the increasing localisation of the mode), one should expect the numerical error to increase with m (which is clear from comparison with solutions on a
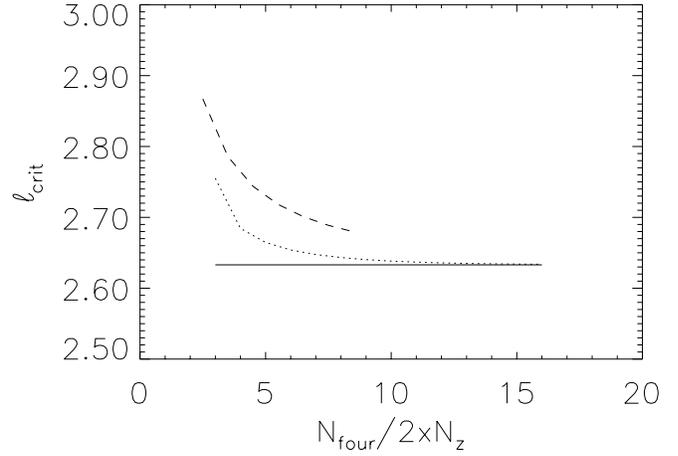

Fig. 3. Convergence graph for the Fourier series (dashed) and the finite element code (dotted). Shown is the marginal stability length as a function of the number of expansion functions used (the number of terms in the Fourier series, or twice the number of gridpoints for the finite element code). The solid horizontal line is the converged result, on which both codes agree.

Table 1. Summary of numerical results from the MALTS code and WKB estimates for equilibrium 3 with $\sigma = 0.15$ and $\lambda = 0.6$.

m	$l_{c,\text{num}}$	$l_{c,\text{WKB}}$	relative error
1	3.219139	3.105242	0.0367
2	2.873549	2.832368	0.0145
3	2.777750	2.741410	0.0133
4	2.729496	2.695931	0.0125
5	2.699152	2.668643	0.0114
10	2.633178	2.614068	0.0071
15	2.609435	2.595877	0.0052
20	2.597366	2.586781	0.0041
25	2.590217	2.581320	0.0034
30	2.585595	2.577685	0.0031
40	2.580084	2.573137	0.0027
50	2.576976	2.570409	0.0026

coarser grid). For example, a convergence study indicates that $m = 1$ has an absolute error of order 10^{-7}, while for $m = 50$ this is up to 10^{-3}. When trying to get a numerical estimate for ℓ_0 and ℓ_1 by assuming an expansion of the form (16) for ℓ and taking only the first three terms, it is difficult to decide which m give the best results: for low m the neglected terms in the WKB expansion are too important, for high m the numerical error is bigger than the $\mathcal{O}(m^{-2})$ term (which also explains why the relative error in the third column does not scale like m^{-2}).

In Fig. 4 it is shown that the radial structure of the eigenmodes for increasing m indeed follows the scaling assumed in the WKB analysis. To demonstrate this we have plotted the cut of the two-dimensional eigenfunction with the plane $z = 0$, as a function of the rescaled coordinate x. Although the values of m used are fairly low, the different eigenfunctions can, as expected, hardly be distinguished. A detailed comparison of the
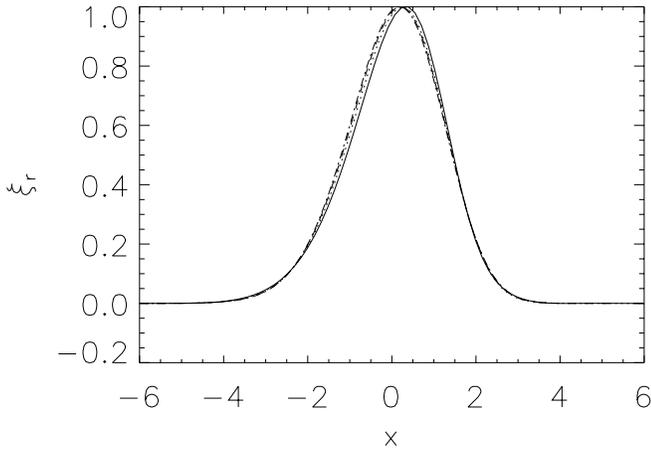
Fig. 4. Radial dependence of the numerical eigenfunctions at $z = 0$ for increasing values of m: 5 (solid line), 10 (dotted), 15 (dashed), 20 (dot-dashed), using the rescaled coordinate $x \equiv m^{1/2}(r - r_0)$. The shift in the eigenfunctions is present because the exact position of the mode localisation also depends on m, with the localisation at r_0 reached for $m \to \infty$
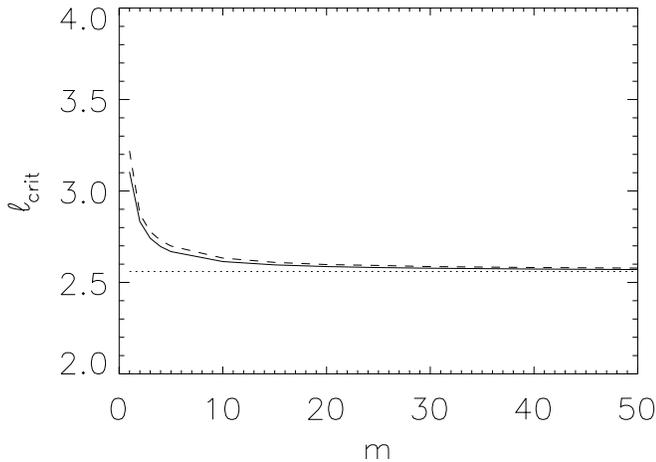

Fig. 5. Marginal stability length as a function of m for $\lambda = 0.6$: numerical (dashed line) versus WKB results (dotted line: ℓ_0 only; solid line: including the contribution from ℓ_1).
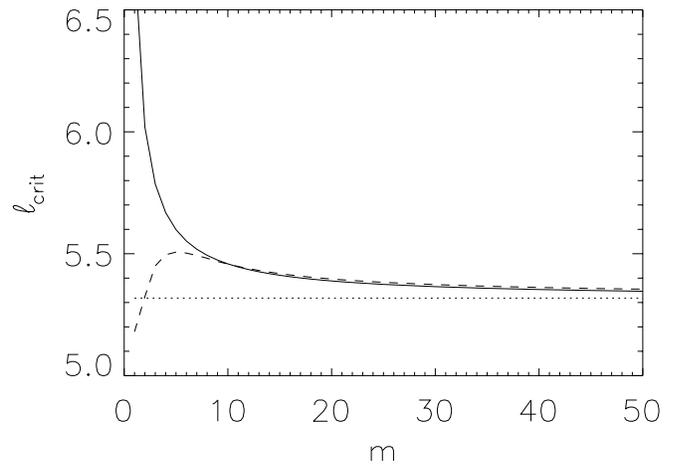

Fig. 6. Marginal stability length as a function of m for $\lambda = 0.8$: numerical (dashed line) versus WKB results (dotted line: ℓ_0 only; solid line: including the contribution from ℓ_1).

eigenfunctions found numerically and that reconstructed from the WKB analysis again yields a perfect match.

The superb agreement between the numerically calculated marginal stability length and the WKB results is most clearly displayed in Figs. 5-8, all using the equilibrium given by Eq. (3) with $\sigma = 0.15$. In Fig. 5 we show how the marginal stability length changes as m is increased, and how the numerical values approach those given by the WKB method ($\lambda = 0.6$ for this graph). It is amazing how close the WKB results are to the actual values, even for low m. Fig. 6 shows the same type of comparison, but now for $\lambda = 0.8$ (which reduces the ratio of gas to magnetic pressure). Again, we find very good agreement for high m (from about $m = 5$ upwards). For very low m the difference has now become much bigger. We also note that while for smaller λ (higher pressure) the marginal stability

length decreases monotonically with m, this is no longer the case in Fig. 6: now the length first increases, reaches a maximum at $m = 5$, and then it again switches to the monotonically decreasing dependence. For $\lambda = 0.8$ we see that the $m = 1$ mode is already the first to become unstable, rather than the $m \to \infty$ mode as for $\lambda = 0.6$. As λ is further increased, which implies the equilibrium is getting closer to its force-free form, the same basic dependence of ℓ on m is found, but the position of the maximum (and thus the switch to the monotonically decreasing behaviour) is shifted to higher values of m. Since the WKB results presented here can only describe this latter form of dependence, this implies that we need to consider higher and higher values of m to obtain good accuracy with the WKB method (but as long as there is a finite pressure gradient, the WKB results remain valid as $m \to \infty$). What actually happens is that at the lower values of m the marginal stability length begins to assume a different form of scaling, one that is typical for force-free and nearly force-free fields. When m is high enough (but not too high), and the equilibrium pressure gradient small enough, these values can be predicted with a different WKB analysis, as we will demonstrate in a subsequent paper dealing specifically with force-free fields.

In Fig. 7 we show the dependence of the marginal stability length on λ for various m (including the WKB value for $m \to \infty$), while in Fig. 8 we compare the numerical values for $m = 10$ with the full WKB results, including the ℓ_1 correction term, over the same range of λ. Again, it is quite striking how well the WKB formulae approximate the critical length, provided the equilibrium is sufficiently far from force-free. Another important conclusion to be drawn from Fig. 5 is that at least for this equilibrium, only two values of m need to be considered to completely determine stability: $m = 1$ and $m \to \infty$. Combining the numerical code to determine the former with the WKB analysis to obtain the latter therefore gives a complete stability analysis of this family of equilibria. In fact, even if it cannot be excluded that for other families of equilibria there
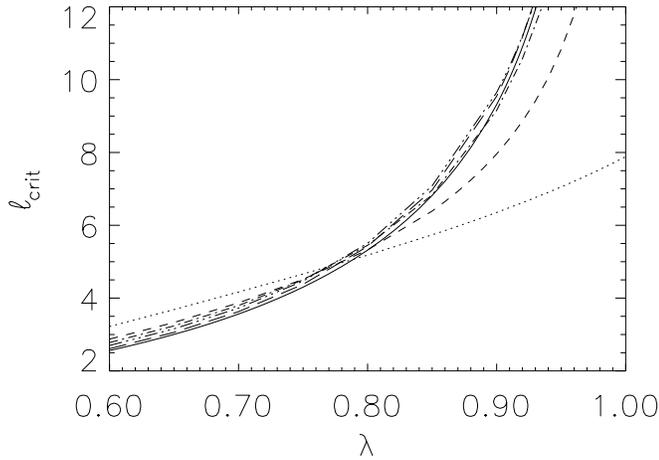
Fig. 7. Marginal stability length as a function of λ, for $m = 1, 2, 3, 5, 15$ (the larger m, the lower the starting value at $\lambda = 0.6$) and $m \to \infty$ (solid line), where the latter is given by ℓ_0 in the WKB analysis.
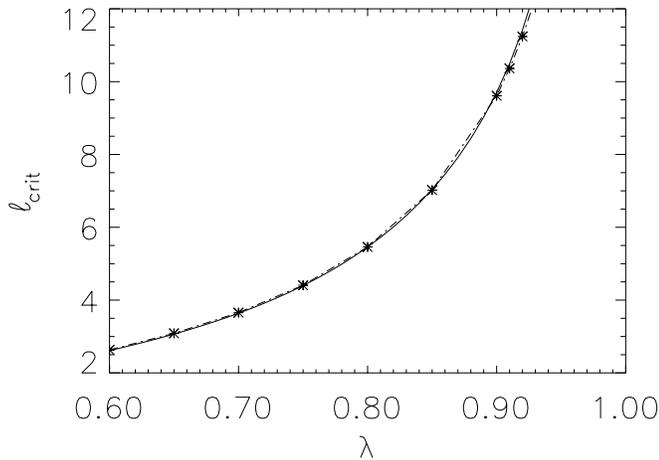

Fig. 8. Critical lengths as a function of λ for $m = 10$. The numerically calculated values are indicated by asterisks (and connected with the dashed line), while the solid line gives the WKB values.

exists a range of pressure where the shortest critical length is found for some other value of m, it is always the case that for sufficiently high pressure the $m \to \infty$ mode is most unstable, while for very low pressure $m = 1$ becomes most unstable. Hence, we only need to consider the other values of m near the point where the critical lengths for these two modes cross over. That, plus the fact that we have a big overlap region of the two methods, means that *we have all the required tools available to perform a very straightforward stability analysis for* any *one-dimensional cylindrically symmetric equilibrium model for a line-tied coronal loop.*

5. Summary and discussion

In this paper we have introduced a combination of a new efficient numerical code and a semi-analytical WKB analysis to study the stability of one-dimensional cylindrically symmetric

equilibrium models of line-tied coronal loops with finite pressure gradients. The numerical code can be used to study modes with low values of the azimuthal wave number m, while the WKB method is applicable for the high wave numbers. We have shown that in a typical family of coronal loop equilibria there is a large region of overlap where both methods have acceptable accuracy. Therefore, the combination of these two methods provides us with *sufficient* tools required to perform a complete stability analysis for any non-force-free 1D model for a line-tied coronal loop. As we have demonstrated that both the $m = 1$ and the $m \to \infty$ modes can be the first to become unstable, depending on the strength of the pressure gradient relative to the magnetic field, both the WKB method and the numerical code are *necessary* in order to be able to determine the true marginal stability point for any non-force-free 1D cylindrical coronal loop model.

On its own, the finding that for sufficiently large pressure gradients the $m \to \infty$ mode is the first to become unstable is important because these high-m modes produce very short length-scales and thus couple very efficiently to dissipative effects like resistivity. This allows the magnetic field to break free from the constraints imposed by the photospheric anchoring (line-tying), and release its stored energy on a fast time-scale, even though the equilibrium has only evolved slightly beyond the ideal marginal stability limit. In the equilibria studied here, the $m \to \infty$ modes are the first to become unstable only for fairly high plasma pressure. At the centre of the loop model the plasma β, i.e. the ratio of gas pressure to magnetic pressure is of order unity, which is much higher than values typical for the solar corona. However, the estimated values of the coronal β are necessarily some form of volume averages. Performing similar averaging in the equilibrium used here reduces the plasma β significantly. Furthermore, the property that $m \to \infty$ modes have shorter marginal stability lengths than low-m modes is related to the size of the pressure gradients rather than the pressure. Thus, it is easy to conceive equilibria with sharp local pressure gradients which still have this property for a realistic *average* plasma β.

The methods described here to determine the ideal stability threshold for all values of m are an invaluable aid to the numerical study of the nonlinear evolution of ideal MHD instabilities. These nonlinear studies are computationally far more expensive, and it is therefore impractical to use the nonlinear equations to determine the stability boundaries. It is far more convenient to first determine linear stability properties for a given type of equilibrium with the methods described in this paper, and then to decide for which cases it would be interesting and relevant to follow the non-linear behaviour. Also, the linear eigenfunctions can be used to determine an initial perturbation that leads to rapid growth, and to estimate the resolution required in the spatial grid.

Once the critical length for the onset of linear instability is determined, the 'free' magnetic energy can be calculated as the volume integral $E_f = \int B_\theta^2 \mathrm{d}V / \mu$. Note that for the equilibrium model considered here the free *magnetic* energy at marginal stability *decreases* as the plasma β increases, because the marginal

stability length is highest when the equilibrium is at its force-free state (see Figs. 7 and 8). However, the (increasing) internal energy also contributes. For a nearly force-free field, taking a typical magnetic field strength of $10 - 100$ Gauss and loop radius of 10^4 km, the free magnetic energy is approximately $10^{24} - 10^{26}$ Joule at the marginal stability length, which is in the range of typical flare energies. Non-linear simulations (Lionello et al., 1998, Arber et al., 1998) indicate that a significant amount of this free energy is released as the instability develops.

In a subsequent paper, we will deal with force-free magnetic equilibria, and demonstrate that there too, the combination of a similar numerical code and a rather different WKB analysis provides a complete stability assessment.

Appendix A: a brief description of the MALTS code

The MALTS code is a new member in a family of codes that solve the linearised MHD equations for 2D equilibria by using a finite element discretisation in both non-ignorable coordinates. For a more extensive description of the use of finite elements in linearised ideal MHD, see Gruber and Rappaz (1985). For the MALTS code we selected bicubic finite elements for the discretisation, i.e. the dependence on r and z coordinates is treated separately using a representation in terms of cubic Hermite finite elements in both coordinates. In practical terms we first select a rectangular, but not necessarily equidistant, $N_r \times N_z$ mesh in the (r,z) domain (in a more advanced application non-rectangular meshes can be accommodated by using isoparametric finite elements). With every mesh point (r_k, z_l) we then associate four local expansion functions formed by combining each of the two cubic Hermite finite element polynomials, h_1 and h_2, in the r coordinate with those in the z coordinate:

$$\left\{ H_{ij}^{kl}(r, z) = h_i^k(r) h_j^l(z) \right\} \text{ for } i, j = 1, 2, \quad \text{(A1)}$$

giving a total of $4 \times N_r \times N_z$ functions. The variables in the marginal stability equations are then written as a linear superposition of all these functions. As is well-known, the expansion in terms of cubic Hermite polynomials has the useful property that it preserves the continuity of the functions and their derivatives. Also, we may expect fourth-order convergence in the mesh size (Zienkiewicz 1971).

As in the WKB analysis, we first redefine the longitudinal coordinate as $z = \ell \bar{z}$ to bring out the unknown quantity ℓ explicitly. After defining the displacement components

$$\xi_1 = r\xi_r, \qquad \xi_2 = \boldsymbol{\xi} \cdot \boldsymbol{B}, \qquad \xi_3 = (\boldsymbol{v} \times \boldsymbol{B})_r, \quad \text{(A2)}$$

and the auxiliary variables

$$y_1 = \frac{\partial v_1}{\partial z}, \qquad y_2 = \frac{\partial v_2}{\partial z}, \qquad y_3 = \frac{\partial v_3}{\partial z}, \quad \text{(A3)}$$

and taking the θ dependence to be of the form $\exp(im\theta)$, we rewrite the components of the marginal stability equation (1) in the form

$$\tilde{\boldsymbol{A}}(\boldsymbol{U}) = \frac{1}{\ell} \tilde{\boldsymbol{B}} \left(\frac{\partial \boldsymbol{U}}{\partial \bar{z}} \right), \quad \text{(A4)}$$

where $\boldsymbol{U}$ is the vector containing the six variables: $\boldsymbol{U}^T = (v_1, v_2, v_3, y_1, y_2, y_3)$, and $\tilde{\boldsymbol{A}}$ and $\tilde{\boldsymbol{B}}$ are operator matrices.

As explained above, we then write all variables as a linear combination of the local bicubic Hermite polynomials H_{ij}^{kl}. To obtain the final set of linear equations for the coefficients in the superposition, we multiply Eq. (A4) with each of the H_{ij}^{kl} and integrate over the (r, z) domain (this amounts to the Galerkin procedure of making the error orthogonal to the function space generated by the expansion functions). To improve accuracy, second order derivatives on the expansion functions are avoided by using integration by parts. The boundary conditions in r and z are imposed by removing those elements that are nonzero at the boundaries from the relevant expansion. The final result is a linear matrix eigenvalue problem of the form

$$A \cdot X = \frac{1}{\ell} B \cdot X, \quad \text{(A5)}$$

where X is the vector containing all the expansion coefficients and A and B are band matrices of order $6 \times 4 \times N_r \times N_z$ (for convenience, B has been made Hermitian). Eq. (A5) can be solved using standard linear algebra algorithms.

Using the numerical code as described above with a mesh of order $N_r \times N_z = 50 \times 25$, adequate solutions are obtained for low values of m (≤ 5), when the eigenfunction has a global character in r and only a small number of oscillations in z. As m becomes large however, the modes are increasingly localised radially and because the most unstable modes are those with the same helicity as the field lines, the number of oscillations in the z coordinate increases rapidly with m (linearly for strongly non-force-free fields, quadratically for nearly force-free). For larger m therefore, accuracy is lost quite rapidly, and the number of gridpoints, particularly in the z coordinate, would have to be increased significantly. But storage requirements for matrices A and B put a strict upper limit on this, while also the CPU time required goes up rapidly. There is fortunately a very easy way of remedying this. While we are only interested in the most unstable mode at present, and we know this must follow the field lines (i.e. have the same helicity), we can explicitly build this property into the eigenfunctions. This is simply done by separating off, as in the WKB analysis, the eikonal factor. We set

$$\boldsymbol{U} = \tilde{\boldsymbol{U}} e^{-imqz}, \quad \text{(A6)}$$

where all the rapid variation of $\boldsymbol{U}$ is captured in the exponential factor, while $\tilde{\boldsymbol{U}}$ describes the slow variation along the field lines. Unfortunately, using Eq. (A6) for sheared magnetic fields (so that $\partial q / \partial r \neq 0$) implies that every radial derivative of one of the variables in $\boldsymbol{U}$ introduces $z = \ell \bar{z}$ explicitly in the equations.

Without additional modifications therefore we would no longer obtain an eigenvalue problem of the form (A5), but instead get

$$A \cdot X = \frac{1}{\ell} B \cdot X + \ell C \cdot X. \tag{A7}$$

This is no longer a 'standard' eigenvalue problem, and special (more costly) algorithms would need to be developed to solve this type of linear algebra problems. We preferred the alternative approach to look for ways to change the method slightly so as to obtain the standard eigenvalue problem (A5) again. A first possibility is to define additional variables (in practice only two are required), e.g. adding the definition

$$\frac{1}{\ell \bar{z}} u_1 = \xi_1, \tag{A8}$$

we can replace all occurrences of $z \xi_1$ in the original equations by u_1, and following the rest of the procedure as described above we obtain the desired result, Eq. (A5), but with larger matrices of order $8 \times 4 \times N_r \times N_z$.

A second alternative is to change the eikonal factor in Eq. (A6) and replace $q(r)$ by q_0, a constant. Here, q_0 must be selected to approximately equal the value of $q(r)$ at the position where the modes localise as m increases. The great advantage of this approach over the first one is that it doesn't require additional variables, and therefore doesn't increase the size of the matrices involved. The down side is that it takes out the anticipated rapid variation in z completely only on one flux surface (near the maximum amplitude), and only part of it on neighbouring surfaces. The further the distance to the 'central' flux surface, the more rapid the variation in z becomes, but fortunately because the eigenmode amplitude decreases exponentially, the impact of this is very small. (In fact this argument is only true for strongly non-force-free fields; somewhat surprisingly we find that for nearly force-free fields and m not too large, the eigenmodes are actually better represented by this radially constant eikonal factor, and it is the original one that introduces rapid variations. This will be discussed in more detail in a subsequent paper dealing specifically with force-free fields.) The optimal value for q_0 can easily be determined from the WKB analysis, or otherwise the best choice can be made by varying q_0 until the minimum length is found (an implicit application of the energy principle). The latter method is actually equivalent to that described by authors using a Fourier series approach (Einaudi and Van Hoven 1983, De Bruyne and Hood 1992), where the wave numbers k_n of the Fourier modes used are shifted by a constant k_0, which is than varied to give the best results.

Since both options discussed above (constant versus non-constant eikonal factor) have their pros and cons, both have been implemented as options into the MALTS code. As it turns out, which of the two methods works best depends on the case under consideration, but they are never dramatically different as to convenience and resources used.

Finally, we should also point out that when the equilibrium gas pressure is identically zero everywhere, only Eqs. (5) and (7) need to be solved (the parallel component η of the displacement vector is no longer present in these). Consequentially this case is implemented as a separate version of the MALTS code using smaller matrices, hence storage and CPU are also much reduced. Otherwise, the options and techniques are the same as those for the non-force-free case.

References

Anzer, U. 1968, Sol. Phys. 3, 298.

Arber, T., Longbottom, A., and Van der Linden, R.A.M., Astrophys. J., in preparation.

Bender, C.M. and Orszag, S.A. 1978, Advanced Mathematical Methods for Scientists and Engineers, McGraw-Hill, New York.

Cargill, P.J., Hood, A.W., and Migliuolo, S. 1986, Astrophys. J. 309, 402.

Connor, J.W., Hastie, R.J., and Taylor, J.B. 1979, Proc. Roy. Soc. London A365, 1.

De Bruyne, P., and Hood, A.W. 1992, Sol. Phys. 142, 87.

Einaudi, G. and Van Hoven, G. 1983, Sol. Phys. 88, 163.

Gruber, R. and Rappaz, J. 1985, Finite Element Methods in Linear Ideal Magnetohydrodynamics, Springer-Verlag, Berlin-New York.

Hood, A.W. 1986, Sol. Phys. 105, 307.

Hood, A.W. 1992, Plasma Phys. & Contr. Fusion 34, 411.

Hood, A.W., De Bruyne, P., Van der Linden, R.A.M., and Goossens, M. 1994, Sol. Phys. 150, 99.

Lionello, R., Velli, M., Einaudi, G., and Mikic, Z. 1998, Astrophys. J. 494, 840.

Newcomb, W. 1960, Ann. Phys. 10, 232.

Van der Linden, R.A.M., Goossens, M., and Kerner, W. 1990, Comp. Phys. Comm. 59, 61.

Van der Linden, R.A.M, and Hood, A.W. 1995, Astron. Astrophys. 299, 912.

Van der Linden, R.A.M., Hood, A.W., and Goedbloed, J.P. 1994, Sol. Phys. 154, 69.

Velli, M. , Einaudi, G., and Hood, A.W. 1990, Astrophys. J. 350, 428.

Zienkiewicz, O.C., 1971, The Finite Element Method in Engineering Science, McGraw-Hill, London.